Chronic Inhibition of ERK1/2 Signaling Improves Disordered Bone and Mineral Metabolism in Hypophosphatemic (*Hyp*) Mice

Martin Y. H. Zhang, Daniel Ranch, Renata C. Pereira, Harvey J. Armbrecht, Anthony A. Portale, and Farzana Perwad

Department of Pediatrics (M.Y.H.Z., A.A.P., F.P.), University of California, San Francisco, San Francisco, California 94143-0748; Department of Pediatrics (D.R.), University of Texas Health Science Center at San Antonio, San Antonio, Texas 78229; Division of Pediatric Nephrology (R.C.P.), David Geffen School of Medicine at the University of California, Los Angeles, Los Angeles, California 90095; and Geriatric Research, Education, and Clinical Center (H.J.A.), St. Louis Veterans Affairs Medical Center, St. Louis, Missouri 63106

The X-linked hypophosphatemic (*Hyp*) mouse carries a loss-of-function mutation in the *phex* gene and is characterized by hypophosphatemia due to renal phosphate (Pi) wasting, inappropriately suppressed 1,25-dihydroxyvitamin D [1,25$(OH)_2$D] production, and rachitic bone disease. Increased serum fibroblast growth factor-23 concentration is responsible for the disordered metabolism of Pi and 1,25$(OH)_2$D. In the present study, we tested the hypothesis that chronic inhibition of fibroblast growth factor-23-induced activation of MAPK signaling in *Hyp* mice can reverse their metabolic derangements and rachitic bone disease. *Hyp* mice were administered the MAPK inhibitor, PD0325901 orally for 4 wk. PD0325901 induced a 15-fold and 2-fold increase in renal 1α-hydroxylase mRNA and protein abundance, respectively, and thereby higher serum 1,25$(OH)_2$D concentrations (115 ± 13 *vs.* 70 ± 16 pg/ml, $P < 0.05$), compared with values in vehicle-treated *Hyp* mice. With PD0325901, serum Pi levels were higher (5.1 ± 0.5 *vs.* 3 ± 0.2 mg/dl, $P < 0.05$), and the protein abundance of sodium-dependent phosphate cotransporter Npt2a, was greater than in vehicle-treated mice. The rachitic bone disease in *Hyp* mice is characterized by abundant unmineralized osteoid bone volume, widened epiphyses, and disorganized growth plates. In PD0325901-treated *Hyp* mice, mineralization of cortical and trabecular bone increased significantly, accompanied by a decrease in unmineralized osteoid volume and thickness, as determined by histomorphometric analysis. The improvement in mineralization in PD0325901-treated *Hyp* mice was confirmed by microcomputed tomography analysis, which showed an increase in cortical bone volume and thickness. These findings provide evidence that in *Hyp* mice, chronic MAPK inhibition improves disordered Pi and 1,25$(OH)_2$D metabolism and bone mineralization. **(*Endocrinology* 153: 1806–1816, 2012)**

The MAPK signaling proteins are ubiquitously expressed in all eukaryotes and regulate highly specific biological responses within cells. Constitutive overactivation of the MAPK signaling pathway is responsible for various human diseases including cancer, neurodegenerative diseases, and developmental defects (1). Small molecule inhibitors that target signaling components within the MAPK pathway have been developed to suppress activity of the pathway and in clinical settings have been used to suppress cell proliferation in patients with cancer (2–6).

X-linked hypophosphatemia (XLH) is an inherited disorder of phosphate (Pi) and vitamin D metabolism (7–10)

ISSN Print 0013-7227 ISSN Online 1945-7170
Printed in U.S.A.

doi: 10.1210/en.2011-1831 Received September 30, 2011. Accepted January 6, 2012.
First Published Online February 14, 2012

Abbreviations: BFR, Bone formation rate; *egr-1*, early growth response-1 gene; EIA, enzyme immunoassay; FGF, fibroblast growth factor; GAPDH, glyceraldehyde-3-phosphate dehydrogenase; Gus, β-glucuronidase; *Hyp*, hypophosphatemic; IR, infrared; MEK, MAPK kinase; microCT, microcomputed tomography; Npt2, sodium-dependent phosphate transport protein 2; 1,25$(OH)_2$D, 1,25-dihydroxyvitamin D; pERK1/2, phosphorylated ERK1/2; PHEX, phosphate-regulating gene with homologies to endopeptidases on the X chromosome; Pi, phosphate; WT, wild type; XLH, X-linked hypophosphatemia.

caused by loss-of-function mutations in the phosphate-regulating gene with homologies to endopeptidases on the X chromosome (*PHEX*) gene (11–13). In patients with XLH and hypophosphatemic (*Hyp*) mice, a mouse model of XLH, the plasma concentration of fibroblast growth factor (FGF)-23 is greatly increased (14–17). In *Hyp* mice, excess circulating FGF-23 induces constitutive activation of MAPK signaling in the kidney and as a consequence, inhibition of renal Pi reabsorption, hypophosphatemia, suppression of renal 1,25-dihydroxyvitamin D [1,25$(OH)_2$D] production, and inappropriately low or normal serum 1,25$(OH)_2$D concentrations (9, 10). The severe hypophosphatemia and 1,25$(OH)_2$D deficiency contribute to the defective skeletal mineralization and growth retardation, which are characteristic features of *Hyp* mice (12, 18–20). The skeletal phenotype of the *Hyp* mouse is characterized by severe kyphosis, rickets, osteomalacia, and shortened hind limbs. Ablation of the *fgf-23* gene in *Hyp* mice results in reversal of the *Hyp* phenotype, providing direct evidence that FGF-23 excess is critical to the pathogenesis of XLH (15, 21). We have shown that MAPK signaling via ERK1/2 is necessary for the suppressive effects of FGF-23 on renal Pi reabsorption and 1,25$(OH)_2$D production (10). Short-term inhibition of MAPK signaling in *Hyp* mice using a specific MAPK kinase (MEK) inhibitor, PD0325901, blocks the renal actions of FGF-23, resulting in increased renal Pi reabsorption and 1,25$(OH)_2$D production (10). However, it is not known whether the abnormal biochemical and skeletal phenotype in *Hyp* mice can be corrected by chronic inhibition of MEK/ERK1/2 signaling.

In this study, we hypothesized that in *Hyp* mice, sustained inhibition of MEK/ERK1/2 signaling will correct the hypophosphatemia and 1,25$(OH)_2$D deficiency and thereby improve the skeletal mineralization defect induced by excess FGF-23. To test this hypothesis, we treated *Hyp* mice with PD0325901 for 4 wk and examined the effect of MEK/ERK1/2 signal inhibition on bone and mineral metabolism.

Materials and Methods

Animals

We studied male C57BL/6J *Hyp* mice and their wild-type littermates, 80–90 d of age, purchased from Jackson Laboratory (Bar Harbor, ME). All mice were fed a constant diet containing 0.6% phosphorus and 1% calcium (Teklad diet 98243; Harlan Laboratories, Madison, WI) starting 4 d before the experiment. To determine the effect of blockade of MEK/ERK1/2 signaling on bone and mineral metabolism, *Hyp* mice were administered the MEK inhibitor, PD0325901, 7.5 mg/kg·dose, or vehicle orally 5 d/wk for 4 wk. In mice and humans, PD0325901 selectively inhibits the activity of MEK, thereby blocking phosphorylation of ERK1/2, the activator kinase immediately downstream of MEK, without blocking phosphorylation of other MAPK (22–24). On d 28, 2 h after administration of the final dose of PD0325901, the mice were anesthetized with ketamine, and blood was obtained for determination of serum calcium, Pi, 1,25$(OH)_2$D, FGF-23, and intact PTH concentrations. The kidneys were removed and frozen for subsequent preparation of total RNA and protein. The femurs were removed for skeletal analysis by microcomputed tomography (microCT) and bone histomorphometry. All procedures were approved by the Committee on Animal Research, University of California, San Francisco.

Serum biochemistry

Serum phosphorus and calcium concentrations were determined using kits from Stanbio Laboratories (San Antonio, TX). Serum 1,25$(OH)_2$D concentrations were determined using an enzyme immunoassay (EIA) kit from Immunodiagnostic Systems, Inc. (Scottsdale, AZ). Serum intact PTH and FGF-23 concentrations were determined using EIA kits from Immutopics International (San Clemente, CA). The mouse FGF-23 (C-Term) EIA kit is a two-site ELISA for the measurement of FGF-23. The antibodies detect epitopes within the carboxyl-terminal (C-Term) region of mouse FGF-23.

Real-time PCR

Total RNA was isolated from kidney and bone using TRIzol reagent (Invitrogen, Carlsbad, CA). cDNA was synthesized using 1× PCR buffer, 7.5 mM $MgCl_2$, 1 mM deoxynucleotide triphosphate, 5 μM random primers, and 2.5 U/liter Moloney murine leukemia virus reverse transcriptase enzyme at the following temperatures: 25 C for 10 min, 48 C for 40 min, and 95 C for 5 min. Probes and primer sets for mouse early growth response-1 gene (*egr-1*) were purchased from Roche (Indianapolis, IN) and for mouse FGF-23 from Applied Biosystems (Foster City, CA). The 1α-hydroxylase, 24-hydroxylase, β-glucuronidase (Gus), sodium-dependent phosphate transport protein 2 (Npt2)-a, and Npt2c probes and primers were custom designed as previously described (10). The mRNA abundance of the gene of interest, expressed relative to that of Gus or glyceraldehyde-3-phosphate dehydrogenase (GAPDH) mRNA, was quantitated by real-time PCR using the ABI 7900 HT sequence detection system (Applied Biosystems) as previously described (25). The threshold cycle (Ct) at which a statistically significant increase in signal above background fluorescence was determined, and the Ct values for the gene of interest were normalized to Ct values for Gus or GAPDH.

Western blot analysis

Mouse kidney total protein (25 μg), renal mitochondrial protein (35 μg), and renal brush border membrane vesicles (25 μg) were isolated (26, 27), fractionated on 8% sodium dodecyl sulfate-polyacrylamide gel and transferred to polyvinyl difluoride membranes as previously described (10). Activation of MAPK signaling in the kidney was determined by detection of phos-

phorylated ERK1/2 (pERK1/2) protein using antiphospho-ERK1/2 monoclonal antibody (Cell Signaling Technology, Danvers, MA) and visualized by chemiluminescence (Supersignal West Dura; Pierce Biotechnology, Rockford, IL). Equal protein loading was determined using a mouse anti-ERK 2 monoclonal antibody (Santa Cruz Biotechnology, Inc., Santa Cruz, CA). For detection of Npt2a, Npt2c, and 1α-hydroxylase proteins, membranes were probed with a rabbit anti-Npt2a polyclonal antibody (1:300) (α Diagnostic International, Inc., San Antonio, TX), rabbit anti-Npt2c polyclonal antibody (1:1000) (Sigma-Aldrich, St. Louis, MO), and rabbit anti-1α-hydroxylase polyclonal antibody (1:1500 dilution, a kind gift from H. J. Armbrecht, St. Louis Veterans Affairs Medical Center, St. Louis, MO), respectively. Equal protein loading was determined using a rabbit anti-β-actin polyclonal antibody (1:5000) (Cell Signaling Technology). The membranes were subsequently blotted using an infrared (IR)-labeled secondary antibody, IRDye 800CW and IRDye 680 (1:25,000) (Li-Cor Biosciences, Lincoln, NE). The bound complex was detected using Odyssey infrared imaging system (LiCor Biotechnology). The images were analyzed using the Odyssey Application Software to obtain the integrated fluorescence intensities from IR detection. The ratio of fluorescence intensities of the protein of interest was normalized to that of the loading control protein and the data were plotted on a bar graph.

Microcomputed tomography

To characterize the skeletal architecture of wild-type (WT) and *Hyp* mice, we performed microCT scans of the femur. Femurs were isolated, fixed in 10% phosphate-buffered formalin for 24 h, and then treated with 70% ethanol. Bones were then scanned in a tube containing 70% ethanol by using a Scanco vivaCT 40 scanner (Scanco Medical, Basserdorf, Switzerland) as previously described (28). To assess trabecular bone in the distal femoral metaphysis, 100 serial cross-sectional scans (1.05 mm) of the secondary spongiosa were obtained from the end of the growth plate, extending proximally with 10.5-μm voxel size and 55-kV x-ray energy. To assess cortical bone, 100 serial cross sections (1.05 mm) of the femur were obtained from the femoral midshaft with 10.5-μm voxel size and 55-kV x-ray energy. For analysis of microCT images, thresholds (350–1000) were applied to distinguish the mineralized bone matrix from soft tissue. Linear attenuation was calibrated with hydroxyapatite as the standard. Image analysis and three-dimensional reconstructions were performed with the manufacturer's software (Scanco Medical).

Bone histomorphometry

Static and dynamic histomorphometry were carried out on WT and *Hyp* mice after 4 wk of treatment with PD0325901. Mice were injected with calcein 20 mg/kg and 15 mg/kg demeclocycline at an interval of 7 and 2 d, respectively. Femurs were dissected, fixed in 70% ethanol, dehydrated, and embedded undecalcified in methyl methacrylate. Longitudinal sections, 5 μm thick, were cut on a microtome (Jung Supercut 2065-Leica; Leica, Heidelberg, Germany) and stained with toluidine blue (pH 6.4). Static parameters of bone formation and resorption were measured in a defined area between 150 and 600 μm from the growth plate, using an OsteoMeasure morphometry system (Osteometrics, Atlanta, GA) (29). For dynamic histomorphometry, mineralizing surface per bone surface and mineral apposition rate were measured in unstained sections under UV light, using a B-2A set long-pass filter consisting of an excitation filter ranging from 450 to 490 nm, a barrier filter at 515 nm, and a dichroic mirror at 500 nm. Bone formation rate (BFR) was calculated. Polarized-light microscopy was used to analyze the orientation of bone collagen fibrils using a polarizer (Nikon, Inc., Melville, NY). The terminology and units used are those recommended by the Histomorphometry Nomenclature Committee of the American Society for Bone and Mineral Research (30). For determination of mineral content and for visualization of cartilage, sections were stained with von Kossa solution and safranin-O as described previously (28).

Statistical analysis

Data are expressed as means ± SEM. The significance of differences between vehicle and treatment groups was analyzed by *t* test or between multiple groups by one-way ANOVA, using Sigma Stat statistical software (Jandel Scientific, San Rafael, CA). *Post hoc* testing was performed using the Student-Newman-Keuls test. $P < 0.05$ was considered statistically significant.

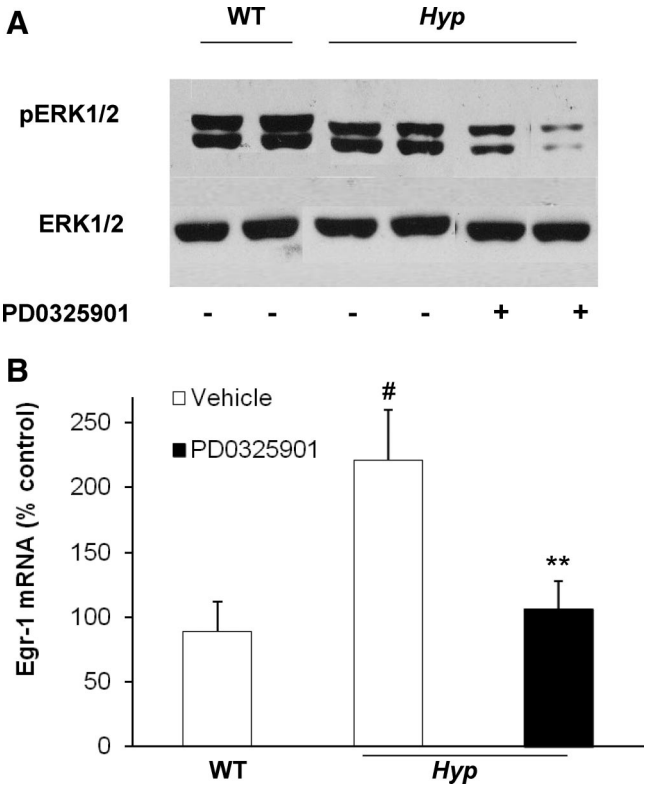

FIG. 1. Chronic inhibition of MAPK signaling in WT and *Hyp* mice. The WT and *Hyp* mice were treated with vehicle or PD0325901 for 4 wk. A, Whole-kidney total protein extracts were probed with rabbit anti-pERK1/2 antibodies (*top panel*). Protein loading was determined using total ERK2 protein (*bottom panel*). B, *Egr-1* mRNA abundance was quantitated by real-time PCR, normalized to that of Gus mRNA, and expressed as a percent relative to vehicle-treated WT mice. *Bars* depict mean ± SEM (n = 6 mice/group). #, $P < 0.05$, compared with WT mice; **, $P < 0.05$, compared with *Hyp* mice treated with vehicle.

Results

Chronic inhibition of MAPK Signaling in *Hyp* mice

We previously demonstrated that in *Hyp* mice, MAPK signaling is constitutively activated in the kidneys, leading to increased expression of *egr-1* (10), an immediate-early response gene encoding a zinc finger transcription factor that is downstream of the MAPK signaling pathway (31, 32). We also showed that acute (4 d) administration of the MEK inhibitor PD0325901 inhibited MAPK signaling by blocking ERK1/2 phosphorylation and decreasing *egr-1* mRNA expression in the kidney (10). In the present study, chronic (4 wk) administration of PD0325901 decreased the abundance of pERK1/2 protein in the kidney of *Hyp* mice (Fig. 1A). In vehicle-treated *Hyp* mice, the abundance of *egr-1* mRNA was 2.5-fold higher than in WT mice, as determined by real-time PCR ($P < 0.05$) (Fig. 1B). In *Hyp* mice, treatment with PD0325901 decreased *egr-1* mRNA abundance by 50% compared with vehicle-treated *Hyp* mice ($P < 0.05$) (Fig. 1) to values not different from those in vehicle-treated WT mice. Gain in body weight during the 4-wk period was not significantly different between WT and *Hyp* mice treated with vehicle (0.93 ± 0.60 *vs.* 0.53 ± 0.34 g, $P = 0.58$). However, in PD0325901-treated *Hyp* mice, gain in body weight was 5-fold greater than in vehicle-treated *Hyp* mice (2.35 ± 0.56 *vs.* 0.53 ± 0.34 g, $P < 0.05$). Survival was 100% in all treatment groups.

Effects of chronic MAPK signaling blockade on serum biochemistries

In vehicle-treated *Hyp* mice, the mean serum Pi concentration was low, and $1,25(OH)_2D$ concentration was inappropriately low for the degree of hypophosphatemia, compared with values in WT mice (Fig. 2, A and C). Compared with vehicle-treated *Hyp* mice, PD0325901 treatment induced a 70% increase in the serum Pi concentration (5.1 ± 0.5 *vs.* 3.0 ± 0.2 mg/dl, $P < 0.05$) and a 64% increase in the serum $1,25(OH)_2D$ concentration (115 ± 13 *vs.* 70 ± 16 pg/ml, $P < 0.05$), the latter to values not different from those in vehicle-treated WT mice. In vehicle-treated *Hyp* mice, the mean serum concentration of calcium was lower, and PTH was higher than values in vehicle-treated WT mice (Fig. 2, B and D). In PD0325901-treated *Hyp* mice, the serum calcium concentration increased (9.5 ± 0.2 *vs.* 8.6 ± 0.2 mg/dl, $P < 0.05$), and the serum PTH concentration decreased greatly compared with values in *Hyp* mice treated with vehicle (75 ± 19 *vs.* 573 ± 210 pg/ml, $P < 0.05$).

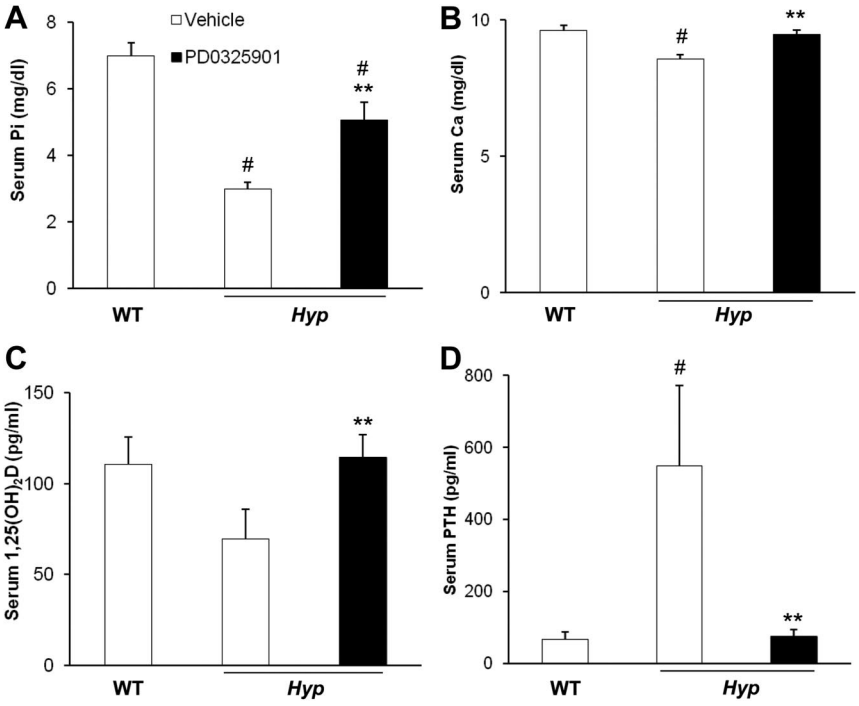

FIG. 2. Effects of chronic MAPK signaling blockade on serum biochemistry. WT and *Hyp* mice were treated with vehicle or PD0325901 for 4 wk. *A*, Serum phosphorus concentrations. *B*, Serum calcium concentrations. *C*, Serum $1,25(OH)_2D$ concentrations. *D*. Serum PTH concentrations. Bars depict mean + SEM (n = 6 mice/group) # $P < 0.05$, compared with WT mice treated with vehicle; ** $P < 0.05$, compared with *Hyp* mice treated with vehicle.

Effects of chronic MAPK signaling blockade on renal $1,25(OH)_2D$ metabolism

To determine the effect of chronic blockade of MAPK signaling on renal $1,25(OH)_2D$ metabolism, we measured the renal abundance of 1α-hydroxylase mRNA by real-time PCR (Fig. 3A). In vehicle-treated mice, 1α-hydroxylase mRNA abundance was 6-fold lower in *Hyp* mice than in WT mice ($P < 0.05$), consistent with the lower serum $1,25(OH)_2D$ concentrations. In PD0325901-treated *Hyp* mice, 1α-hydroxylase mRNA increased by 15-fold ($P < 0.05$) compared with values in vehicle-treated *Hyp* mice and was 2-fold higher than values observed in WT mice. The renal abundance of 24-hydroxylase mRNA was significantly increased in vehicle-treated *Hyp* mice compared with WT mice ($P < 0.05$) and decreased after treatment with PD0325901 in *Hyp* mice ($P < 0.05$) (Fig. 3B). Western blot analysis revealed that treatment with PD0325901

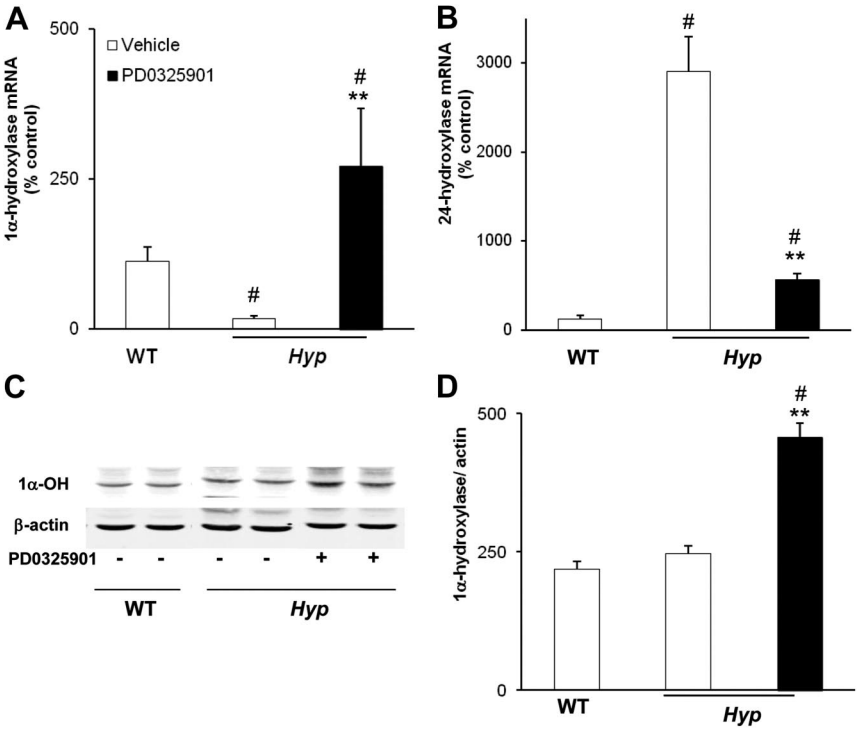

FIG. 3. Effects of chronic MAPK signaling blockade on renal 1,25(OH)$_2$D metabolism. WT and *Hyp* mice were treated with vehicle or PD0325901 for 4 weeks. A, Renal 1α-hydroxylase mRNA abundance was quantitated by real-time PCR, normalized to that of Gus mRNA, and expressed as a percent relative to vehicle-treated WT mice. B, Renal 24-hydroxylase mRNA abundance was quantitated as above. C and D, Renal mitochondrial 1α-hydroxylase protein abundance was normalized to β-actin (for Western blotting, n = 1 mouse/lane). *Bars* depict mean ± SEM (n = 6 mice/group). #, $P < 0.05$, compared with WT mice treated with vehicle; **, $P < 0.05$, compared with *Hyp* mice treated with vehicle.

induced an almost 2-fold increase in renal mitochondrial 1α-hydroxylase protein compared with the vehicle-treated group ($P < 0.05$) (Fig. 3, C and D).

Effects of chronic MAPK signaling blockade on renal Pi metabolism

In the proximal tubule, FGF-23 suppresses renal Pi reabsorption by down-regulating the expression of sodium-dependent Pi cotransporters, Npt2a and Npt2c (33, 34). To determine the effect of chronic blockade of MAPK signaling on renal Pi metabolism, we measured renal mRNA abundance of Npt2a and Npt2c in vehicle- and PD0325901-treated mice. In vehicle-treated mice, renal Npt2a mRNA abundance was 58% lower in *Hyp* than in WT mice ($P < 0.05$) (Fig. 4A). In *Hyp* mice treated with PD0325901, Npt2a mRNA abundance increased by 22% compared with that in *Hyp* mice treated with vehicle, although the change was not statistically significant ($P = 0.13$, Fig. 4A). In vehicle-treated mice, Npt2a brush border protein abundance was lower in *Hyp* than in WT mice, as expected (Fig. 4B). Treatment with PD0325901 induced a 4-fold increase in Npt2a brush border protein abundance ($P < 0.05$) compared with vehicle-treated *Hyp* mice; the value was significantly higher than that observed in vehicle-treated WT mice ($P < 0.05$) (Fig. 4C). Renal Npt2c mRNA abundance was 49% lower in *Hyp* mice than in WT mice ($P < 0.05$) (Fig. 4A) and did not change significantly after treatment with PD0325901. Npt2c brush border protein abundance was lower in *Hyp* than in WT mice, as expected (Fig. 4B) and decreased further with PD0325901 treatment, although the change was not statistically significant.

Skeletal analysis by microCT

We examined the skeletal structure of the femoral bones of WT and *Hyp* mice by microCT analysis. Compared with WT mice, *Hyp* mice have short femurs and widened epiphyses with poor preservation of bone micro architecture, particularly at the distal metaphysis. Bone matrix is undermineralized, consistent with osteomalacia (Fig. 5). Quantitative analysis of cortical bone at the femoral midshaft shows that bone volume is 40% lower, thickness is 53% lower, and porosity is 60% higher than values in WT mice ($P < 0.05$, Supplemental Table 1). Treatment with PD0325901 resulted in a 5% increase in femoral length (11.79 ± 0.15 *vs.* 11.21 ± 0.36 mm, $P = 0.13$) that was accompanied by a 15% increase in cortical bone volume ($P < 0.05$, Supplemental Table 1) and 22% increase in cortical thickness ($P < 0.05$, Supplemental Table 1) compared with values in vehicle-treated *Hyp* mice. As expected, cortical porosity decreased significantly in PD0325901-treated *Hyp* mice compared with the vehicle-treated *Hyp* mice ($P < 0.05$, Supplemental Table 1).

Skeletal analysis by bone histomorphometry

We performed histomorphometric analysis of the secondary spongiosa of the distal femoral metaphysis in WT and *Hyp* mice (Table 1). The characteristic finding of rickets induced by a mineralization defect was evident in vehicle-treated *Hyp* mice: widened epiphyses, disruption of the growth plate, and substantially large areas of unmineralized osteoid when compared with WT mice (Fig. 6). Total trabecular bone volume was 2.5 fold lower in *Hyp* mice and osteoid bone volume was 100-fold higher and was associated with a 12-fold increase in osteoid thickness $P < 0.05$, Table 1). *Hyp* mice also showed a significantly

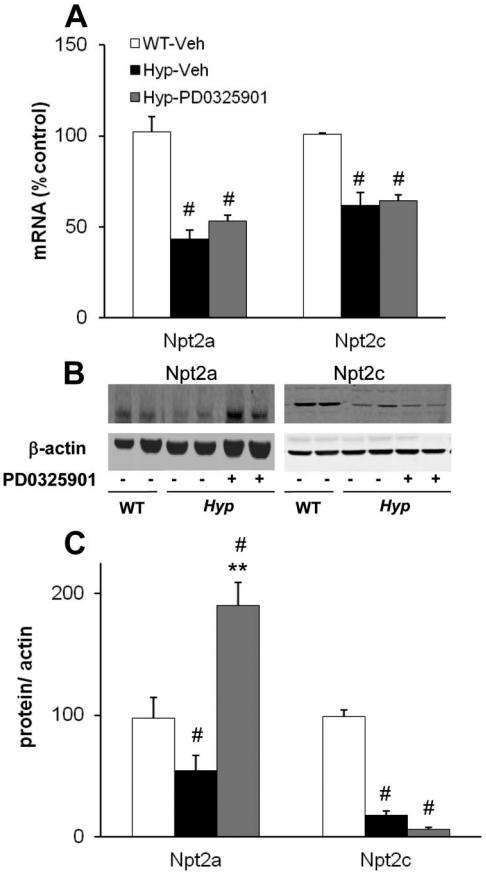

FIG. 4. Effects of chronic MAPK signaling blockade on renal Pi metabolism. WT and *Hyp* mice were treated with vehicle or PD0325901 for 4 wk. A, Renal Npt2a and Npt2c mRNA abundance was quantitated by real-time PCR, normalized to that of Gus mRNA and expressed as a percent relative to vehicle-treated WT mice. B and C, Renal brush border Npt2a and Npt2c protein abundance normalized to β-actin (for Western blotting, samples were pooled from two mice per lane). *Bars* depict mean ± SEM [n = 3 pooled samples (six mice per condition)]. #, $P < 0.05$, compared with WT mice treated with vehicle; **, $P < 0.05$, compared with *Hyp* mice treated with vehicle.

higher trabecular separation and lower trabecular number indicating diminished osteoblast function. The *Hyp* mice femurs were poorly mineralized in both trabecular and cortical bone sections consistent with osteomalacia (Fig. 6). In all the *Hyp* mice in the vehicle-treated group, kinetic parameters of mineralization (*i.e.* bone formation rates and mineral apposition rates) were not measurable due to poor mineralization activity (Fig. 6 and Table 1).

Treatment of *Hyp* mice with PD0325901 significantly decreased osteoid volume and thickness in both trabecular and cortical bone ($P < 0.05$, Table 1 and Fig. 6) when compared with the vehicle-treated group. The decrease in osteoid volume was accompanied by a significant increase in areas of mineralized osteoid in cortical and trabecular regions (Fig. 6). The mineralization parameters, bone formation rate, mineral apposition rate, and mineralizing surfaces were detectable in three of six treated mice and were significantly improved compared with vehicle-treated *Hyp* mice. There was no significant change in trabecular number or separation in PD0325901-treated mice compared with vehicle-treated *Hyp* mice (Table 1). Although osteoblast and osteoclast surfaces trended up, these parameters did not change significantly.

To determine the effect of PD0325901 on the growth plate, we examined the histology of primary spongiosa in the distal femoral metaphysis. By comparison with WT mice, the metaphyseal growth plate of *Hyp* mice is severely disorganized and the columnar structure of the chondrocytes is absent (Fig. 6). As a result, the growth plate is widened and disrupted with an increase in unmineralized osteoid in the primary spongiosa, as shown by decreased areas of von Kossa staining. Treatment of *Hyp* mice with PD0325901 did not affect the disorganized growth plate structure but did substantially improve mineral deposition in the distal metaphysis. PD0325901-treated *Hyp* mice show increased areas of calcified bone in the growth plate and femoral midshaft compared with the areas of unmineralized osteoid in the vehicle-treated *Hyp* mice (Fig. 6).

Effects of chronic MAPK signaling blockade Fgf-23 production

To determine the effect of PD0325901 on FGF-23 production in *Hyp* mice, we determined *fgf-23* mRNA expression in bone and measured serum FGF-23 concentrations. PD0325901 treatment induced a 4-fold increase in *fgf-23* mRNA abundance in femoral bone and a 2.5-fold increase in serum FGF-23 concentration compared with values in vehicle-treated *Hyp* mice ($P < 0.05$) (Fig. 7).

Discussion

In the present study, we provide evidence that MAPK signaling via MEK/ERK1/2 plays a critical role in the pathogenesis of disordered renal Pi transport, vitamin D metabolism, and bone mineralization in *Hyp* mice. We demonstrate that sustained inhibition of FGF-23-dependent MEK/ERK1/2 signaling corrects the aberrant renal Pi transport and $1,25(OH)_2D$ deficiency and is associated with marked improvement in the mineralization defect, which is the characteristic skeletal abnormality seen in *Hyp* mice. The present study is the first to show that a MAPK signaling inhibitor can be used *in vivo* in mice to treat an inherited disorder of bone and mineral metabolism caused by impaired renal Pi reabsorption and $1,25(OH)_2D$ synthesis. Previous studies in *Hyp* mice have shown that supplementation with Pi and $1,25(OH)_2D$ is sufficient to correct their mineralization defect and improve skeletal growth (35–37). Therefore, we attribute the

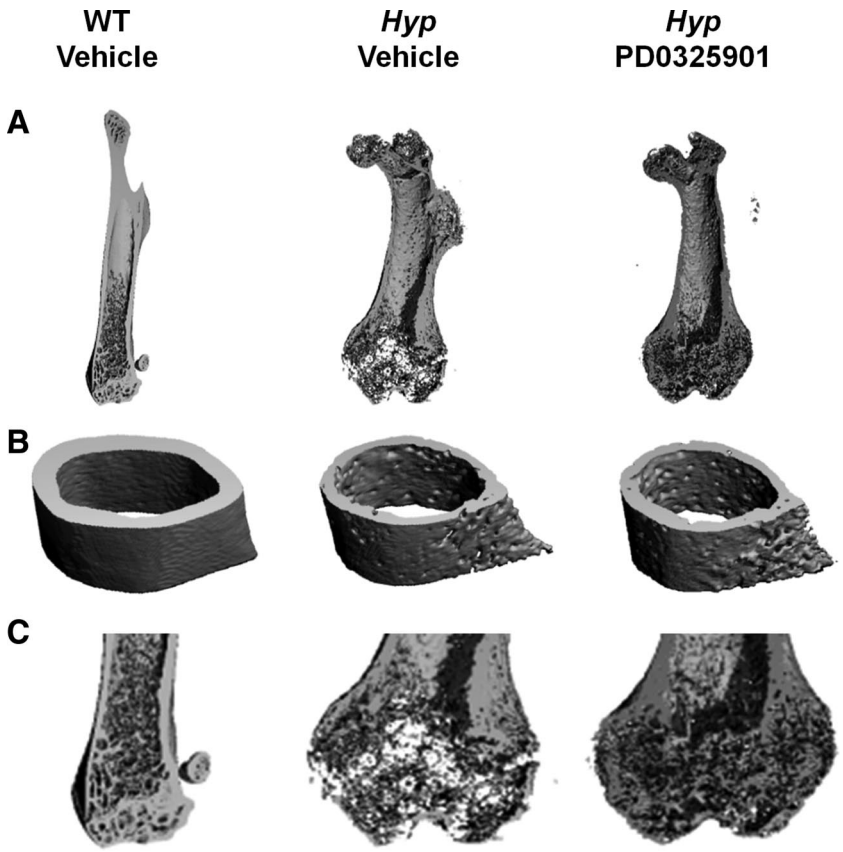

FIG. 5. Three-dimensional microCT representation of the femur in WT and *Hyp* mice after treatment with vehicle or PD0325901 for 4 wk. A, Axial sections of the entire femur. B, Cross-sectional images of the cortical midshaft. C, Axial sections of the distal femur (enlarged).

improvement in skeletal mineralization in *Hyp* mice to the correction of impaired renal Pi reabsorption and $1,25(OH)_2D$ production.

FGF-23 is known to suppress renal $1,25(OH)_2D$ production by down-regulating renal 1α-hydroxylase gene expression and up-regulating 24-hydroxylase gene expression (25, 34, 38, 39). Chronic treatment of *Hyp* mice with PD0325901 induced a substantial increase in the serum $1,25(OH)_2D$ concentration, which can be attributed to the up-regulation of renal 1α-hydroxylase mRNA and protein expression and down-regulation of renal 24-hydroxylase mRNA. These findings provide evidence that sustained inhibition of FGF-23-dependent MEK/ERK1/2 signaling corrects the aberrant renal $1,25(OH)_2D$ synthesis in *Hyp* mice. Treatment of *Hyp* mice with PD0325901 increased serum Pi concentration to a mean value that was 70% of that in WT mice. The increase in serum Pi concentration induced by PD0325901 is due in part to a 4-fold increase in the abundance of Npt2a cotransporter in the renal brush border membrane. These findings suggest that FGF-23-dependent MEK/ERK1/2 signaling regulates membrane trafficking of Npt2a cotransporter in the proximal renal tubule, similar to the actions of PTH (40).

The failure of chronic MEK/ERK1/2 blockade to fully correct the hypophosphatemia in *Hyp* mice, despite full correction of $1,25(OH)_2D$ production, was also seen in our prior study in which PD0325901 was administered for only 4 d (10). These findings suggest that FGF-23 differentially regulates serum Pi and $1,25(OH)_2D$ concentrations, as is also suggested by studies in double-mutant $Fgf23^{-/-}$/*Hyp* mice (15). *Hyp* mice bearing a homozygous $Fgf23^{-/-}$ mutation demonstrate absent circulating FGF-23 and substantially increased serum Pi and $1,25(OH)_2D$ concentrations when compared with *Hyp* mice with an intact *fgf-23* gene (15). In contrast, *Hyp* mice bearing a heterozygous $Fgf23^{+/-}$ mutation demonstrate a 50% reduction in serum FGF-23 concentration, normal serum $1,25(OH)_2D$ concentration, but persistent hypophosphatemia and skeletal abnormalities when compared with *Hyp* mice with an intact *fgf-23* gene. Our findings parallel those seen in the heterozygous $Fgf23^{+/-}$/*Hyp* mice. These observations suggest that renal $1,25(OH)_2D$ production is more susceptible to suppression by a given dose or circulating concentration of FGF-23 than is renal Pi reabsorption. The mechanism for such differential regulation by FGF-23 is unknown. It is also possible that FGF-23-induced suppression of renal Pi reabsorption depends on activation of other signaling pathways in addition to the MEK/ERK1/2 pathway, and such pathways are not blocked by PD0325901. This possibility is suggested by our finding that renal Npt2c protein expression remained suppressed in *Hyp* mice, despite treatment with PD0325901, and such suppression may have contributed to the persistent hypophosphatemia in these mice. However, we found no evidence for constitutive activation of the p38 (10) or the phosphoinositide 3-kinase pathway in *Hyp* mice (data not shown), pathways that are known to be activated by FGF-23 *in vitro* (41, 42).

In a prior study, we showed that short-term (4 d) treatment of *Hyp* mice with PD0325901 resulted in increased renal Pi reabsorption and $1,25(OH)_2D$ production (10). When that study is compared with the current study of chronic (4 wk) MEK inhibition, we find that most of the changes in mineral metabolism were similar in direction but variable in magnitude, with a few exceptions (10). In

TABLE 1. Bone histomorphometry of the secondary spongiosa in the distal femur.

	WT	*Hyp*	
Parameters	**Vehicle**	**Vehicle**	**PD0325901**
T.Ar	2.86±0.12	3.04±0.13	2.88±0.10
BV/TV (%)	12.76±1.25	5.07±0.53[a]	3.99±0.66
OV/BV (%)	0.73±0.20	73.67±3.7[a]	24.34±2.28[b]
O.Th (μm)	1.53±0.27	18.42±1.06[a]	7.83±0.65[b]
Tb.Th (μm)	33.14±1.45	37.19±1.69	42.63±3.94
Tb.Sp (μm)	233.35±15.20	751.87±111.42[a]	1328.31±436.00
Tb.N (per mm)	3.81±0.22	1.36±0.13[a]	1.01±0.19
MS/BS (%)	8.01±1.62	ND	0.55±0.30[b]
MS/OS (%)	115.45±1.16	ND	0.82±0.40[b]
MAR (μm/dia)	0.74±0.03	ND	0.40±0.04[b]
BFR/BS($\mu m^3/\mu m^2$·yr)	22.54±5.24	ND	1.66±0.46[b]
Mlt	2.22±0.61	ND	1493.81±357.98[b]
OS/BS (%)	7.16±0.90	65.20±2.76[a]	62.90±3.91
Ob.S/BS (%)	4.84±1.32	2.08±0.62	3.93±2.27
ES/BS (%)	4.10±0.31	0.86±0.28[a]	1.50±0.47
Oc.S/BS (%)	1.44±0.21	0.39±0.10[a]	0.56±0.27
N.Ob/T.Ar (per mm)	21.80±5.63	3.77±1.31[a]	3.62±1.07
N.Ob/B.Pm	3.51±0.84	1.91±0.65	4.02±2.43
N.Oc/T.Ar (per mm)	2.84±0.41	0.39±0.07[a]	0.45±0.17

Results are expressed as mean ± SEM (n = 6 mice per group). T.Ar, Trabecular area; BV/TV, bone volume/tissue volume; OV/BV, osteoid volume/bone volume; O.Th, osteoid thickness; Tb.Th, trabecular thickness; Tb.Sp, trabecular separation; Tb.N, trabecular number; MS/BS, mineralizing surface/bone surface; MS/OS, mineralizing surface/osteoid surface; MAR, mineral apposition rate; BS, bone surface; Mlt, mineralization lag time; OS/BS, osteoid surface/bone surface; Ob.S/BS, osteoblast surface/bone surface; ES/BS, eroded surface/bone surface; Oc.S/BS, osteoclast surface/bone surface; N.Ob/T.Ar, number osteoblast/tissue area; N.Ob/B.Pm, number osteoblast/bone perimeter; N.Oc/T.Ar, number osteoclast/tissue area; ND, not determined (unable to measure).

[a] $P < 0.05$, compared with WT mice treated with vehicle.

[b] $P < 0.05$, compared with *Hyp* mice treated with vehicle.

both studies, serum Pi and $1,25(OH)_2D$ concentrations increased significantly. However, serum PTH and calcium concentrations were different at baseline in the two studies; in the short-term study, vehicle-treated *Hyp* mice were normocalcemic and had PTH values that were lower than those in WT mice, whereas in the chronic study, *Hyp* mice were hypocalcemic and had higher PTH values than those in the WT mice. Serum PTH concentrations increased in *Hyp* with short-term PD0325901 treatment but were suppressed with chronic PD0325901 treatment, relative to values in vehicle-treated *Hyp* mice. Whether differences in the baseline characteristics in the vehicle-treated mice contributed to the different PTH response in the treated animals in the two studies will require further investigation.

The skeletal mineralization defect in *Hyp* mice is attributed to hypophosphatemia, $1,25(OH)_2D$ deficiency, and an intrinsic osteoblast defect that impairs mineralization of the osteoid matrix (12, 18, 43). In vehicle-treated *Hyp* mice, poor mineralization of the femoral bone was evident on microCT scan and bone histomorphometry when compared with WT mice, consistent with previous reports (15, 44, 45). PD0325901 treatment induced significant increases in cortical bone volume and thickness and a marked decrease in unmineralized osteoid volume and thickness. These changes reflect increased mineralization of the osteoid matrix, as demonstrated by von Kossa staining; these increases can be attributed to the correction of Pi, calcium, and $1,25(OH)_2D$ deficiency. A limitation of this study is that MEK inhibition was initiated in 12- to 13-wk-old *Hyp* mice, an age when the clinical features of hypophosphatemic rickets are well established. It is possible that treatment of younger *Hyp* mice or longer duration of treatment with PD0325901 would be more effective in improving skeletal growth and in reversing their skeletal defects. This possibility is supported by observations that supplementation with Pi and $1,25(OH)_2D$ in older *Hyp* mice markedly improved bone mineralization but failed to completely correct the osteomalacia (37). The failure to fully correct the bone histomorphometry parameters may also be due, in part, to incomplete correction of hypophosphatemia, alternate signaling pathways not blocked by PD0325901, or an intrinsic osteoblast defect induced by the *phex* mutation that is not corrected by systemic MEK/ERK1/2 signal inhibition. The latter possibility is supported by the finding that overexpression of the *phex* gene in *Hyp* mice led to partial rescue of their skeletal abnormalities despite no improvement in hy-

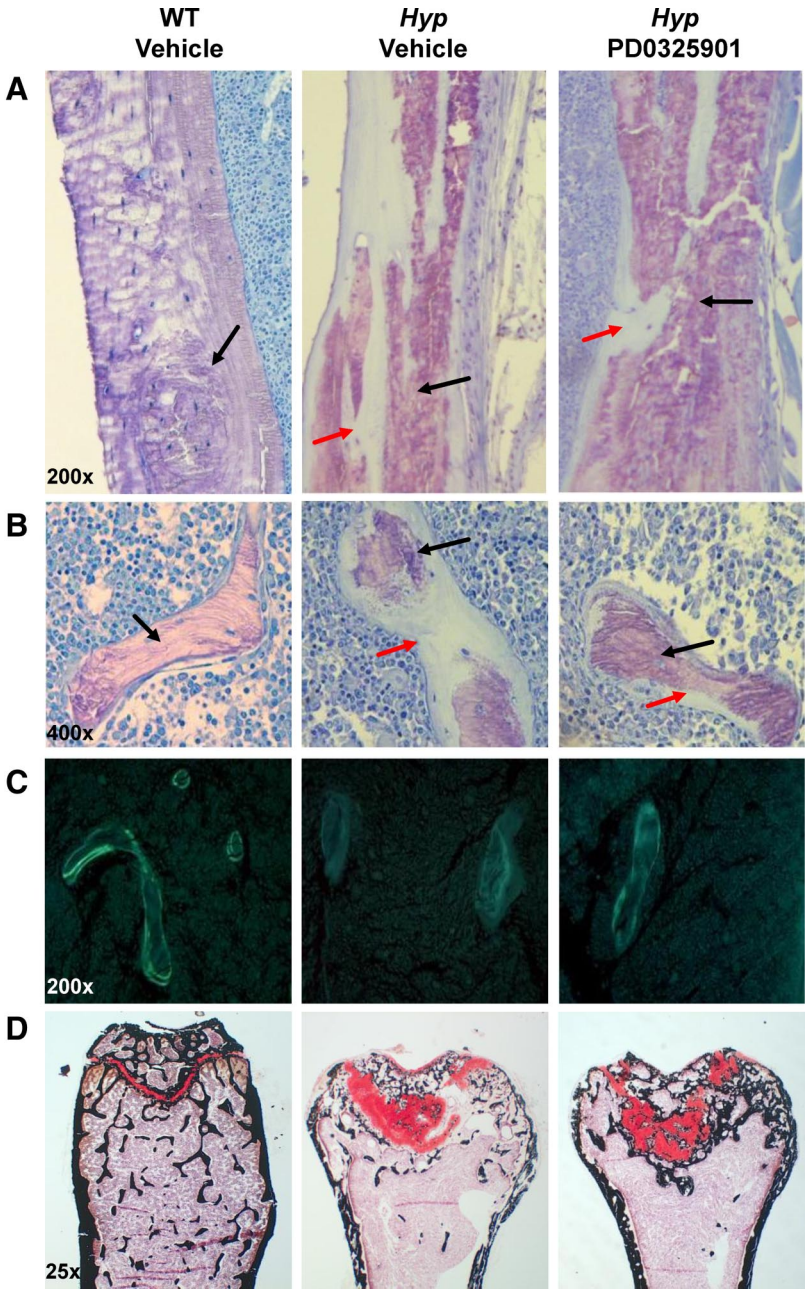

FIG. 6. Histological analysis of the distal femur of WT and *Hyp* mice after treatment with vehicle or PD0325901 for 4 wk. Undecalcified sections were visualized by toluidine blue stain [*purple* indicates mineralized bone (*black arrow*); *light blue* indicates unmineralized osteoid (*red arrow*)]. A, Cortical bone section of the distal femoral metaphysis (×200 magnification). B, Trabecular bone section of the distal femoral metaphysis (×400 magnification). C, Unstained cross-sections of the femur visualized under UV illumination. Quantification of fluorochrome-labeled surfaces were performed and data were used to calculate mineral apposition rate and BFR (×200 magnification). D. Histological analysis of the growth plate at the distal femoral metaphysis in WT and *Hyp* mice. Plastic sections of the distal growth plate visualized by safranin O (*red staining* indicates cartilage) and calcified areas visualized by von Kossa (*black staining*) (×25 magnification).

pophosphatemia or $1,25(OH)_2D$ deficiency (46–49). However, although expression of mutant *phex* in bone may contribute independently to the mineralizing defect in *Hyp mice*, treatment with anti-FGF-23 antibodies can rescue the *Hyp* phenotype despite the persistent *phex* mutation (50), suggesting that complete blockade of FGF-23 actions is sufficient to correct the abnormal biochemical and skeletal phenotype in *Hyp* mice.

In wild-type mice, systemic administration of an inhibitor of all FGF receptors induced an increase in serum $1,25(OH)_2D$ and Pi concentrations (51). Such pan-FGF receptor inhibition induced a substantial decrease in *fgf-23* mRNA expression in bone and thereby a decrease in serum FGF-23 concentrations. Thus, systemic FGF receptor blockade resulted in suppression of *fgf-23* production in bone. In contrast, the present study shows that in *Hyp* mice, MEK blockade with PD0325901 is associated with an increase in bone *fgf-23* mRNA expression and in serum FGF-23 concentrations in *Hyp* mice. Therefore, the improvement in renal Pi and $1,25(OH)_2D$ metabolism in our study is due to inhibition of FGF-23 signaling in the kidney and not due to a decrease in circulating FGF-23 concentration. Whether PD0325901 directly affects skeletal mineralization in *Hyp* mice is unknown and will require further investigation.

In summary, the results of the present study provide evidence that in *Hyp* mice, sustained inhibition of FGF-23-induced MEK/ERK1/2 signaling in the kidney normalizes serum $1,25(OH)_2D$ concentrations by stimulating renal $1,25(OH)_2D$ synthesis and partially corrects the hypophosphatemia by increasing renal Pi reabsorption via Npt2a. The resultant improvement in mineral homeostasis contributes to the marked improvement in skeletal mineralization, demonstrating the physiological importance of MAPK signaling in the pathogenesis of the *Hyp* phenotype.

Acknowledgments

We thank the Bone Imaging Core/University of California, San Francisco, Endocrine Research Unit, San Francisco-Veterans Affairs Medical Center for microCT data collection and analysis.

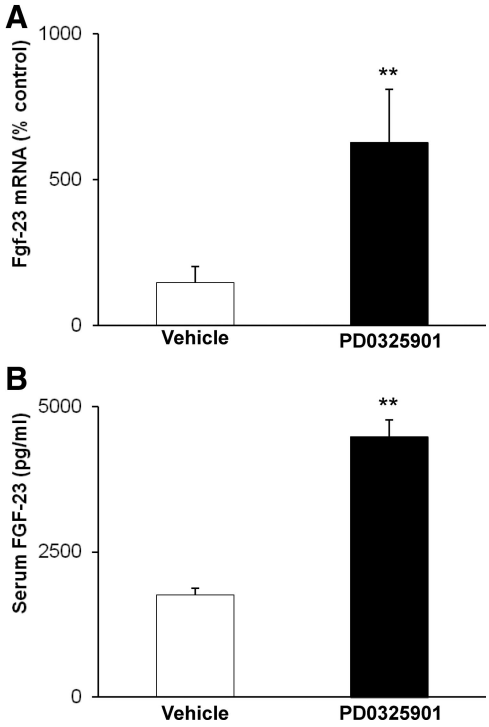

FIG. 7. Effects of chronic MAPK signaling blockade on *fgf-23* production. *Hyp* mice were treated with vehicle or PD0325901 for 4 wk. A, Bone *fgf-23* mRNA abundance was quantitated by real-time PCR, normalized to that of GAPDH mRNA, and expressed as a percent relative to vehicle-treated *Hyp* mice. B, Serum FGF-23 concentrations. *Bars* depict mean ± SEM (n = 6 mice/group). **, $P < 0.05$, compared with *Hyp* mice treated with vehicle.

Address all correspondence and requests for reprints to: Farzana Perwad, M.D., Division of Pediatric Nephrology, Department of Pediatrics, University of California, San Francisco, 533 Parnassus Avenue, U-585, Box 0748, San Francisco, California 94143-0748. E-mail: perwadf@peds.ucsf.edu.

This work was supported by National Institutes of Health Grants DK-073092 and University of California, San Francisco, Academic Senate Grant (to F.P.), a Veterans Affairs merit grant from the Department of Veterans Affairs Research and Development (to H.J.A.), and the Pediatric Nephrology Innovative Research Fund (to A.P.).

Disclosure Summary: The authors have nothing to disclose.

References

1. **Johnson GL, Dohlman HG, Graves LM** 2005 MAPK kinase kinases (MKKKs) as a target class for small-molecule inhibition to modulate signaling networks and gene expression. Curr Opin Chem Biol 9:325–331
2. **Hong DS, Cabanillas ME, Wheler J, Naing A, Tsimberidou AM, Ye L, Waguespack SG, Hernandez M, El Naggar AK, El Naggar AK, Bidyasar S, Wright J, Sherman SI, Kurzrock R, Busaidy NL** 2011 Inhibition of the Ras/Raf/MEK/ERK and RET kinase pathways with the combination of the multikinase inhibitor sorafenib and the farnesyltransferase inhibitor tipifarnib in medullary and differentiated thyroid malignancies. J Clin Endocrinol Metab 96:997–1005
3. **Gilmartin AG, Bleam MR, Groy A, Moss KG, Minthorn EA, Kulkarni SG, Rominger CM, Erskine S, Fisher KE, Yang J, Zappacosta F, Annan R, Sutton D, Laquerre SG** 2011 GSK1120212 (JTP-74057) is an inhibitor of MEK activity and activation with favorable pharmacokinetic properties for sustained in vivo pathway inhibition. Clin Cancer Res 17:989–1000
4. **LoRusso PM, Krishnamurthi SS, Rinehart JJ, Nabell LM, Malburg L, Chapman PB, DePrimo SE, Bentivegna S, Wilner KD, Tan W, Ricart AD** 2010 Phase I pharmacokinetic and pharmacodynamic study of the oral MAPK/ERK kinase inhibitor PD-0325901 in patients with advanced cancers. Clin Cancer Res 16:1924–1937
5. **Lauchle JO, Kim D, Le DT, Akagi K, Crone M, Krisman K, Warner K, Bonifas JM, Li Q, Coakley KM, Diaz-Flores E, Gorman M, Przybranowski S, Tran M, Kogan SC, Roose JP, Copeland NG, Jenkins NA, Parada L, Wolff L, Sebolt-Leopold J, Shannon K** 2009 Response and resistance to MEK inhibition in leukaemias initiated by hyperactive Ras. Nature 461:411–414
6. **Lyubynska N, Gorman MF, Lauchle JO, Hong WX, Akutagawa JK, Shannon K, Braun BS** 2011 A MEK inhibitor abrogates myeloproliferative disease in Kras mutant mice. Sci Transl Med 3:76ra27
7. **Portale AA, Miller WL** 2003 Rickets due to hereditary abnormalities of vitamin D synthesis or action. In: Glorieux FH, Pettifor JM, Juppner H, eds. Pediatric bone. San Diego: Academic Press; 583–598
8. **Brame LA, White KE, Econs MJ** 2004 Renal phosphate wasting disorders: clinical features and pathogenesis. Semin Nephrol 24: 39–47
9. **Farrow EG, Summers LJ, Schiavi SC, McCormick JA, Ellison DH, White KE** 2010 Altered renal FGF23-mediated activity involving MAPK and Wnt: effects of the Hyp mutation. J Endocrinol 207: 67–75
10. **Ranch D, Zhang MY, Portale AA, Perwad F** 2011 Fibroblast growth factor-23 regulates renal $1,25(OH)_2D$ and phosphate metabolism via the MAP kinase signaling pathway in Hyp mice. J Bone Miner Res 26:1883–1890
11. **Tenenhouse HS** 1999 X-linked hypophosphataemia: a homologous disorder in humans and mice. Nephrol Dial Transplant 14:333–341
12. **Tenenhouse HS, Econs MJ** 2001 Mendelian hypophosphatemias. In: Scriver CR, Beaudet AL, Sly WS, Vale D, eds. The metabolic and molecular basis of inherited disease. New York: McGraw Hill; 5039–5068
13. **Rowe PS, Oudet CL, Francis F, Sinding C, Pannetier S, Econs MJ, Strom TM, Meitinger T, Garabedian M, David A, Macher MA, Quesitaux E, Popowska E, Pronicka E, Read AP, Mokrzycki A, Glorieux FH, Drezner MK, Hanauer A, Lenrach H, Goulding JN, O'Riordan JL** 1997 Distribution of mutations in the PEX gene in families with X-linked hypophosphataemic rickets (HYP). Hum Mol Genet 6:539–549
14. **Jonsson KB, Zahradnik R, Larsson T, White KE, Sugimoto T, Imanishi Y, Yamamoto T, Hampson G, Koshiyama H, Ljunggren O, Oba K, Yang IM, Miyauchi A, Econs MJ, Lavigne J, Jüppner H** 2003 Fibroblast growth factor 23 in oncogenic osteomalacia and X-linked hypophosphatemia. N Engl J Med 348:1656–1663
15. **Liu S, Zhou J, Tang W, Jiang X, Rowe DW, Quarles LD** 2006 Pathogenic role of Fgf23 in Hyp mice. Am J Physiol Endocrinol Metab 291:E38–E49
16. **Liu S, Tang W, Zhou J, Stubbs JR, Luo Q, Pi M, Quarles LD** 2006 Fibroblast growth factor 23 is a counter-regulatory phosphaturic hormone for vitamin D. J Am Soc Nephrol 17:1305–1315
17. **Weber TJ, Liu S, Indridason OS, Quarles LD** 2003 Serum FGF23 levels in normal and disordered phosphorus homeostasis. J Bone Miner Res 18:1227–1234
18. **Eicher EM, Southard JL, Scriver CR, Glorieux FH** 1976 Hypophosphatemia: mouse model for human familial hypophosphatemic (vitamin D-resistant) rickets. Proc Natl Acad Sci USA 73:4667–4671
19. **Meyer Jr RA, Gray RW, Meyer MH** 1980 Abnormal vitamin D metabolism in the X-linked hypophosphatemic mouse. Endocrinology 107:1577–1581
20. **Delvin EE, Glorieux FH** 1981 Serum 1,25-dihydroxyvitamin D con-

centrations in hypophosphatemic vitamin D-resistant rickets. Calcif Tissue Int 33:173–175
21. **Sitara D, Razzaque MS, Hesse M, Yoganathan S, Taguchi T, Erben RG, Jüppner H, Lanske B** 2004 Homozygous ablation of fibroblast growth factor-23 results in hyperphosphatemia and impaired skeletogenesis, and reverses hypophosphatemia in Phex-deficient mice. Matrix Biol 23:421–432
22. **Brown AP, Carlson TC, Loi CM, Graziano MJ** 2007 Pharmacodynamic and toxicokinetic evaluation of the novel MEK inhibitor, PD0325901, in the rat following oral and intravenous administration. Cancer Chemother Pharmacol 59:671–679
23. **Bain J, Plater L, Elliott M, Shpiro N, Hastie CJ, McLauchlan H, Klevernic I, Arthur JS, Alessi DR, Cohen P** 2007 The selectivity of protein kinase inhibitors: a further update. Biochem J 408:297–315
24. **Cohen P** 2002 Protein kinases—the major drug targets of the twenty-first century? Nat Rev Drug Discov 1:309–315
25. **Perwad F, Zhang MY, Tenenhouse HS, Portale AA** 2007 Fibroblast growth factor 23 impairs phosphorus and vitamin D metabolism *in vivo* and suppresses 25-hydroxyvitamin D-1α-hydroxylase expression *in vitro*. Am J Physiol Renal Physiol 293:F1577–F1583
26. **Zhang MY, Wang X, Wang JT, Compagnone NA, Mellon SH, Olson JL, Tenenhouse HS, Miller WL, Portale AA** 2002 Dietary phosphorus transcriptionally regulates 25-hydroxyvitamin D-1α-hydroxylase gene expression in the proximal renal tubule. Endocrinology 143:587–595
27. **Biber J, Stieger B, Stange G, Murer H** 2007 Isolation of renal proximal tubular brush-border membranes. Nat Protoc 2:1356–1359
28. **Chang W, Tu C, Chen TH, Bikle D, Shoback D** 2008 The extracellular calcium-sensing receptor (CaSR) is a critical modulator of skeletal development. Sci Signal 1:ra1
29. **Gazzerro E, Pereira RC, Jorgetti V, Olson S, Economides AN, Canalis E** 2005 Skeletal overexpression of gremlin impairs bone formation and causes osteopenia. Endocrinology 146:655–665
30. **Parfitt AM, Drezner MK, Glorieux FH, Kanis JA, Malluche H, Meunier PJ, Ott SM, Recker RR** 1987 Bone histomorphometry: standardization of nomenclature, symbols, and units. Report of the ASBMR Histomorphometry Nomenclature Committee. J Bone Miner Res 2:595–610
31. **Lim CP, Jain N, Cao X** 1998 Stress-induced immediate-early gene, egr-1, involves activation of p38/JNK1. Oncogene 16:2915–2926
32. **Guha M, O'Connell MA, Pawlinski R, Hollis A, McGovern P, Yan SF, Stern D, Mackman N** 2001 Lipopolysaccharide activation of the MEK-ERK1/2 pathway in human monocytic cells mediates tissue factor and tumor necrosis factor α expression by inducing Elk-1 phosphorylation and Egr-1 expression. Blood 98:1429–1439
33. **Larsson T, Marsell R, Schipani E, Ohlsson C, Ljunggren O, Tenenhouse HS, Jüppner H, Jonsson KB** 2004 Transgenic mice expressing fibroblast growth factor 23 under the control of the α1(I) collagen promoter exhibit growth retardation, osteomalacia and disturbed phosphate homeostasis. Endocrinology 145:3087–3094
34. **Shimada T, Urakawa I, Yamazaki Y, Hasegawa H, Hino R, Yoneya T, Takeuchi Y, Fujita T, Fukumoto S, Yamashita T** 2004 FGF-23 transgenic mice demonstrate hypophosphatemic rickets with reduced expression of sodium phosphate cotransporter type IIa. Biochem Biophys Res Commun 314:409–414
35. **Ecarot B, Glorieux FH, Desbarats M, Travers R, Labelle L** 1992 Effect of dietary phosphate deprivation and supplementation of recipient mice on bone formation by transplanted cells from normal and X-linked hypophosphatemic mice. J Bone Miner Res 7:523–530
36. **Marie PJ, Travers R, Glorieux FH** 1982 Healing of bone lesions with 1,25-dihydroxyvitamin D3 in the young X-linked hypophosphatemic male mouse. Endocrinology 111:904–911
37. **Marie PJ, Travers R, Glorieux FH** 1982 Bone response to phosphate and vitamin D metabolites in the hypophosphatemic male mouse. Calcif Tissue Int 34:158–164
38. **Shimada T, Hasegawa H, Yamazaki Y, Muto T, Hino R, Takeuchi Y, Fujita T, Nakahara K, Fukumoto S, Yamashita T** 2004 FGF-23 is a potent regulator of vitamin D metabolism and phosphate homeostasis. J Bone Miner Res 19:429–435
39. **Shimada T, Mizutani S, Muto T, Yoneya T, Hino R, Takeda S, Takeuchi Y, Fujita T, Fukumoto S, Yamashita T** 2001 Cloning and characterization of FGF23 as a causative factor of tumor-induced osteomalacia. Proc Natl Acad Sci USA 98:6500–6505
40. **Biber J, Hernando N, Forster I, Murer H** 2008 Regulation of phosphate transport in proximal tubules. Pflugers Arch 18:77–84
41. **Yamashita T, Konishi M, Miyake A, Inui K, Itoh N** 2002 Fibroblast growth factor (FGF)-23 inhibits renal phosphate reabsorption by activation of the mitogen-activated protein kinase pathway. J Biol Chem 277:28265–28270
42. **Medici D, Razzaque MS, DeLuca S, Rector TL, Hou B, Kang K, Goetz R, Mohammadi M, Kuro-O M, Olsen BR, Lanske B** 2008 FGF-23-Klotho signaling stimulates proliferation and prevents vitamin D-induced apoptosis. J Cell Biol 182:459–465
43. **Liu S, Tang W, Zhou J, Vierthaler L, Quarles LD** 2007 Distinct roles for intrinsic osteocyte abnormalities and systemic factors in regulation of FGF23 and bone mineralization in Hyp mice. Am J Physiol Endocrinol Metab 293:E1636–E1644
44. **Li H, Martin A, David V, Quarles LD** 2011 Compound deletion of Fgfr3 and Fgfr4 partially rescues the Hyp mouse phenotype. Am J Physiol Endocrinol Metab 300:E508–E517
45. **Brownstein CA, Zhang J, Stillman A, Ellis B, Troiano N, Adams DJ, Gundberg CM, Lifton RP, Carpenter TO** 2010 Increased bone volume and correction of HYP mouse hypophosphatemia in the Klotho/HYP mouse. Endocrinology 151:492–501
46. **Liu S, Guo R, Tu Q, Quarles LD** 2002 Overexpression of Phex in osteoblasts fails to rescue the Hyp mouse phenotype. J Biol Chem 277:3686–3697
47. **Erben RG, Mayer D, Weber K, Jonsson K, Jüppner H, Lanske B** 2005 Overexpression of human PHEX under the human β-actin promoter does not fully rescue the Hyp mouse phenotype. J Bone Miner Res 20:1149–1160
48. **Bai X, Miao D, Panda D, Grady S, McKee MD, Goltzman D, Karaplis AC** 2002 Partial rescue of the Hyp phenotype by osteoblast-targeted PHEX (phosphate-regulating gene with homologies to endopeptidases on the X chromosome) expression. Mol Endocrinol 16:2913–2925
49. **Boskey A, Frank A, Fujimoto Y, Spevak L, Verdelis K, Ellis B, Troiano N, Philbrick W, Carpenter T** 2009 The PHEX transgene corrects mineralization defects in 9-month-old hypophosphatemic mice. Calcif Tissue Int 84:126–137
50. **Aono Y, Yamazaki Y, Yasutake J, Kawata T, Hasegawa H, Urakawa I, Fujita T, Wada M, Yamashita T, Fukumoto S, Shimada T** 2009 Therapeutic effects of anti-FGF23 antibodies in hypophosphatemic rickets/osteomalacia. J Bone Miner Res 24:1879–1888
51. **Wöhrle S, Bonny O, Beluch N, Gaulis S, Stamm C, Scheibler M, Müller M, Kinzel B, Thuery A, Brueggen J, Hynes NE, Sellers WR, Hofmann F, Graus-Porta D** 2011 FGF receptors control vitamin D and phosphate homeostasis by mediating renal FGF-23 signaling and regulating FGF-23 expression in bone. J Bone Miner Res 26: 2486–2497